Front. Struct. Civ. Eng. 2023, 17(11): 1723–1738
https://doi.org/10.1007/s11709-023-0948-z

RESEARCH ARTICLE

Drainage design combining drain holes and pinholes for tunnel boring machine segments subject to high water pressure

Yao LU[a], Ming HUANG[a*], Zhijie CHEN[a], Zisheng ZENG[a], Yuchuan LIU[a], Guangzhao DU[b]

[a] *College of Civil Engineering, Fuzhou University, Fuzhou 350108, China*
[b] *Urban Rail Branch, China Railway 11th Bureau Group Co., Ltd., Wuhan 430071, China*
[*] *Corresponding author. E-mail: huangming05@fzu.edu.cn*

ABSTRACT Balance of the groundwater and ecology is crucial for controlled discharge. However, regarding the segments of tunnel boring machines (TBMs) under high water pressure, the stability of the lining structure is often reduced by excessive drain holes required to achieve this balance. The large discharge of pinholes can easily have severe consequences, such as the lowering of the groundwater table, drying of springs, and vegetation wilting. Thus, in this study, according to the fluid–structure coupling theory, a new drainage design for TBM segments was developed by considering a mountain tunnel subject to a high water pressure as a case study. The evolution characteristics, including the external water pressure of the lining, discharge volume of the segment, and groundwater-table drawdown, were investigated via numerical modeling with drain holes and pinholes. The results indicated that the optimal design parameters of drainage segments for the project case were as follows: a circumferential spacing angle and longitudinal number on one side of a single ring of 51° and 2, respectively, for the drain holes and an inclination angle and length of 46.41° and 0.25 times the grouting thickness, respectively, for the pin holes.

KEYWORDS TBM segment, high water pressure, drain hole, pinhole, groundwater table drawdown

1 Introduction

Tunnels are often constructed in mountain areas and buried underground subject to high water pressures [1,2]. Rather than assessment focusing only on the safety and reliability of the project, the effects of tunnel construction on the groundwater environment have attracted increasing attention [3]. For example, the monitoring data of the hydrochemical changes in previous studies revealed that excessive tunnel discharge during construction and operation can cause lowering of the groundwater table [4] and even drying of springs [5,6] and wilting of vegetation [7]. An interactive relationship exists between the tunnel construction and the groundwater environment, as shown in Fig. 1. Additionally, the groundwater environment will affect the tunnel project [8]. For instance, a sudden increase in groundwater inflow of 670 t/d was experienced during tunneling in a limestone formation approximately 53 m below the ground surface [9]. It caused a maximum of 23 mm of ground settlement and severe damage to adjacent structures. According to the literature, various evaluation methods of the groundwater hazard have been used, and meaningful results have been obtained. A model using the analytic hierarchy process and the fuzzy Delphi method was proposed for assessing the classification of tunnel sites from the viewpoint of the groundwater hazard [10]. Using numerical and stochastic models, the hydrogeological hazards for a tunnel structure resulting from the groundwater table rising were evaluated [11,12]. Using a novel deep learning-based model, lining defects such as groundwater leakage and cracks were automatically detected in complex tunnel backgrounds [13].

To solve the problem of the segment discharge for mountain tunnels under high groundwater pressure, the controlled drainage method is feasible [5,14]. Its principle

Article history: Received Aug 27, 2022; Accepted Dec 3, 2022

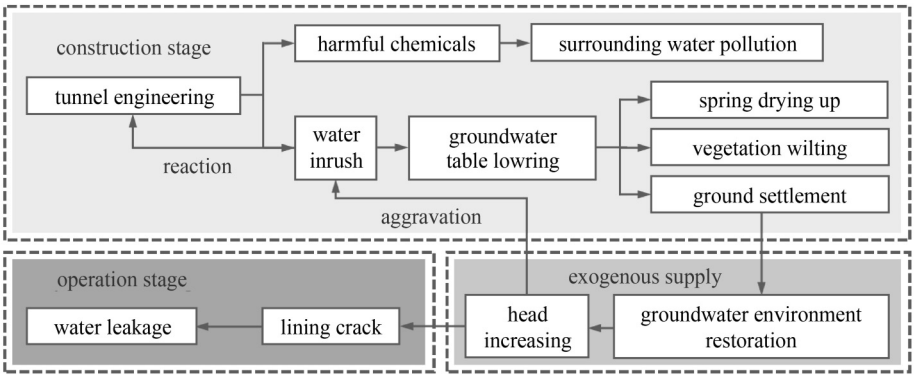

Fig. 1 Interaction between tunnel engineering and the groundwater environment.

is to clog water inflow via the grouting method or other measures and to discharge the parts of seepage behind the composite lining through the inner drainage system for the drilling and blasting tunnels [6]. Tunnel boring machines (TBMs) have become the preferred choice for tunneling, owing to their advantages of high degrees of automation and informatization, high construction efficiency, and good safety [15,16]. The segmental lining of TBM tunnels is usually entirely clogged. Thus, the groundwater discharge and pressure reduction are considered in the drainage design of TBM segments.

A parametric study was performed to optimize the installation and arrangement of the pinhole drainage system for the typical urban underground railway tunnel in Korea [17]. Subsequently, through both material and model tests, the anchored applicability of pinholes, which allow pore water to enter tunnels, was investigated for the fracture zones in subsea tunnels [18]. Taking the Xianglushan diversion tunnel as an example, the effects of the lining, grouting layer, and pinholes on the seepage pressure between the surrounding rock and the lining were analyzed using a custom numerical software [19]. Additionally, a structural type of TBM segment with drain holes was proposed for solving the high-water pressure problem in railway tunnels [20]. Through theoretical analysis, numerical simulation, and model tests, successively, the effects of the discharge volume, number of drain holes, grouting, and surrounding rock conditions on the water pressure outside the lining were investigated [20–22]. For an inclined shaft project in Qilianta Coal Mine, the application effect of drain holes was examined [23]. The foregoing studies indicate that fluid–structure coupling modeling is useful for analyzing the evolution law of the groundwater environment under different parameters of pinholes and drain holes. However, considering the pressure-reducing effect and lining stability, there is a limit to the number of drain holes [19]. The discharge volume of pinholes tends to be excessive, which can have severe consequences, as previously mentioned [5,14].

Therefore, in this study, a novel drainage design for TBM segments was developed via a fluid–structure coupling analysis based on a numerical method. Firstly, taking a mountain tunnel with a 250 m overburden under high water pressure as a case study, the evolution characteristics of drain holes and pinholes were investigated with respect to the external water pressure and discharge volume of the segmental lining, as well as steady drawdown of the groundwater table. Subsequently, the optimal arrangements of drain holes (e.g., lateral section and longitudinal direction) and pinholes (e.g., length and inclination angle) were obtained. Finally, a new drainage segment combing the advantages of drain holes and pinholes was designed, with consideration of the balance between the groundwater and ecology [5].

2 Design method for new drainage segments of tunnel boring machines for tunnels under high water pressure

The design with only one drain hole (i.e., $n_\theta = 1$) in the circumferential direction of TBM segments is called the circumferential single-hole drainage type (see Fig. 2(a)) [21]. The hole is usually located at the arch bottom, where the seepage water can be directly discharged from the ditches on both sides of the invert through drain holes at the inclination angle θ_h. This design is only suitable for tunnels under low water pressures, because of the inability to reduce the water pressure outside the lining in the entire ring area [23]. Regarding circumferential multi-hole drainage segments, the two most common types are double-hole ($n_\theta = 2$; inclination angles of 45° and 135°; see Fig. 2(b)) and triple-hole ($n_\theta = 3$; inclination angles of 45°, 90°, and 135°; see Fig. 2(c)). Compared with the circumferential single-hole type, they allow a more uniform reduction of the external water pressure of the lining. However, the holes at θ_{h2} and θ_{h3}, which are usually connected to the discharge system inside the segment (see Fig. 2(d)), are difficult to dredge in time once the system is blocked. Through the investigation presented in Subsubsection 3.2.1, a more significant

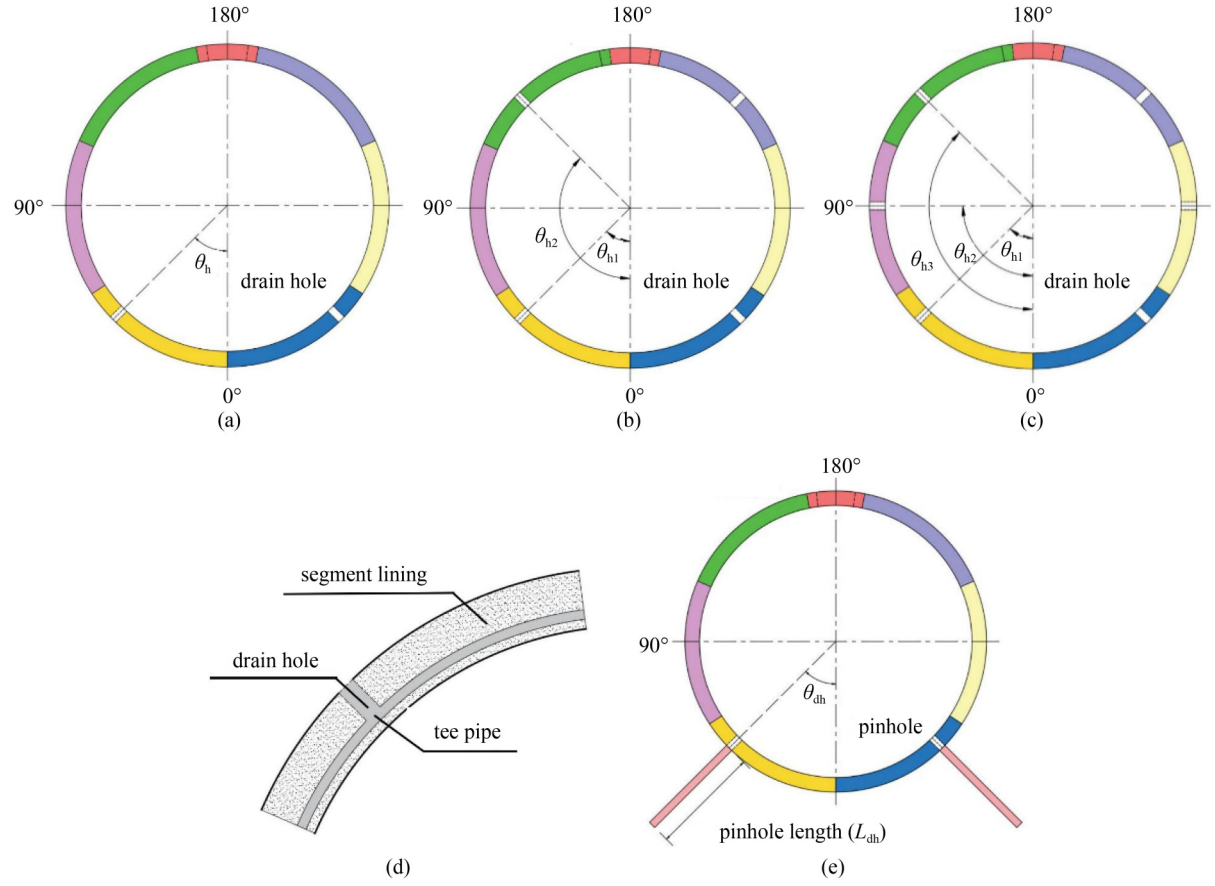

Fig. 2 (a) Single-hole drainage type; (b) double-hole drainage type; (c) triple-hole drainage type; (d) inner drain system of multi-hole drainage types; (e) pinhole drainage type.

pressure-reducing effect on the water pressure outside of the arch spandrel, haunch, and bottom was realized by double-hole and triple-hole types. The applicable tunnel water pressure correspondingly increases. However, the number of drain holes is limited to ensure the stability of the lining structure and the average discharge efficiency of the holes.

A significant depressurizing effect was achieved via pin holes (see Fig. 2(e)) according to the fluid–solid analysis results presented in Subsubsection 3.2.2. A reduction in the number of holes is beneficial for the structural stability, as described previously. The pinholes are often located in the grouting area and close to the arch bottom, which ensures the rapid discharge of groundwater from the ditches on the inner sides of tunnels. However, a large amount of groundwater in the upper part of tunnel rings cannot be discharged in time. Thus, the single-hole drainage type is only suitable for controlled-discharge tunnels under moderate water pressures.

Thus, single-hole drainage-type TBM segments often do not satisfy the discharge requirements for tunnels under high water pressures. For the first time, the advantages of the two types were combined in this study. The design process is shown in Fig. 3. The circumferential external water pressure in the lower area of the tunnel rings is controlled by arranging pinholes near the arch bottom. Additionally, drain holes are arranged between the haunch and crown to control the external water pressure in the upper area. On one hand, the groundwater near pinholes can be quickly discharged through the tunnel ditches. On the other hand, other groundwater can be diverted and discharged through multiple drain holes. Thus, the risk of groundwater accumulation behind the upper lining is significantly reduced.

Many factors affect the discharge and depressurization for the drainage segment, i.e., the thickness of the grouting ring and the angle and number of holes along the longitudinal and circumferential directions of the TBM segments [19,23]. Larger pinholes are more effective for reducing the pore water pressure, and an inverse correlation was established [17,18]. Using the analytical method presented in Subsection 3.1, the optimal ratios of the pinhole length, tunnel radius, and thickness of the grouting ring were determined. Considering the foregoing influencing factors, the external water pressure and discharge volume of the segmental lining and the groundwater-table drawdown were employed to evaluate the discharge and pressure-reducing effects [5,22,24].

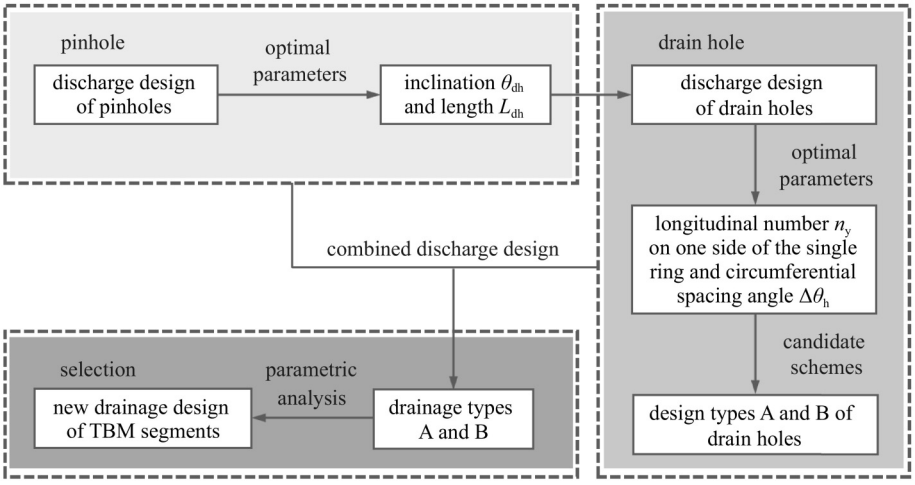

Fig. 3 Design flowchart for the new type of drainage segment.

3 Fluid–structure coupling analysis of different drainage types

3.1 Numerical model

3.1.1 Mountain tunnel

Taking a mountain tunnel on the south-east coast of China as a project case (see Fig. 4(a)), a tunnel ring (see Fig. 4(b)) consists of one key segment (Segment F), two adjacent segments (Segment L), and four standard segments (Segment B), which are prefabricated with concrete of strength grade C55. The impermeability grade is determined by the maximum water pressure that a standard concrete specimen aged 28 d can withstand when tested according to the standard testing method. As described in Ref. [25], the impermeability grade of concrete is divided into six grades: P4, P6, P8, P10, P12, and > P12. The impermeability grade in the present case was determined to be P12. The outer diameter, inner diameter, wall thickness, and ring width were 8300, 7500, 400, and 1800 mm, respectively. The dimensions of the segmental lining are shown in Fig. 4(c). The distance between the groundwater table and the arch crown of the tunnel ring and the overburden pressure were set as 250 m and 1.3 MPa, respectively. The lithology of the fault fracture zone (i.e., the surrounding rock) was tuff, and the rock mass was weathered and broken. The groundwater environment in this section is significantly affected by tunnel construction.

3.1.2 Numerical modeling

The Abaqus software was used to develop a three-dimensional model. Considering the wide influence range of the seepage field, the distance between the side wall of the unlined tunnel and the model boundary was taken as approximately 20 times the tunnel diameter. The model had dimensions of 350 m (width), 3.6 m (length), and 350 m (height), and the mesh was divided as shown in Fig. 5(a). To increase the efficiency of the numerical analysis, only the longitudinal two-ring segments of the model were taken for numerical analysis (see Fig. 5(b)), and the top of the model was taken as the groundwater-table line. The lateral displacement boundaries were fixed in the normal direction. The displacement boundaries at the bottom were fixed in the horizontal, longitudinal, and vertical directions [26]. The ground surface boundaries were free and permeable, at which the initial pore water pressure was 0. The left and right sides of the model were the boundaries of the constant head, where the pore water pressure increased linearly with an increase in height. After excavation, the inner surface of the unlined tunnel was set as the free seepage boundary. After segmental construction, the inner surface of the drain holes was set as the free seepage boundary. The numerical model included the fault fractured zone, grouting ring, TBM segment, and holes, as shown in Fig. 5(a). The Mohr–Coulomb constitutive model was adopted for the surrounding rock and grouting ring. The elastic constitutive model was used for the segment and the drain holes and pinholes (see Fig. 5(c)). The reduced integration element C3D8P, which is the pore-pressure element considering the fluid–solid coupling effect in Abaqus, was used for model meshing.

3.1.3 Determination of parameters

Using the axisymmetric method, an analytical solution for the seepage field of the mountain tunnel grouted radially was derived. It is suitable for tunnels with a buried depth larger than the water head. The water inflow Q_f is expressed as follows:

$$Q_f = \frac{2\pi k_m H_w}{\frac{k_m}{k_s}\ln\frac{r_1}{r_0} + \frac{k_m}{k_i}\ln\frac{r_2}{r_1} + \frac{k_m}{k_g}\ln\frac{r_g}{r_2} + \ln\frac{H_w}{r_g}}, \quad (1)$$

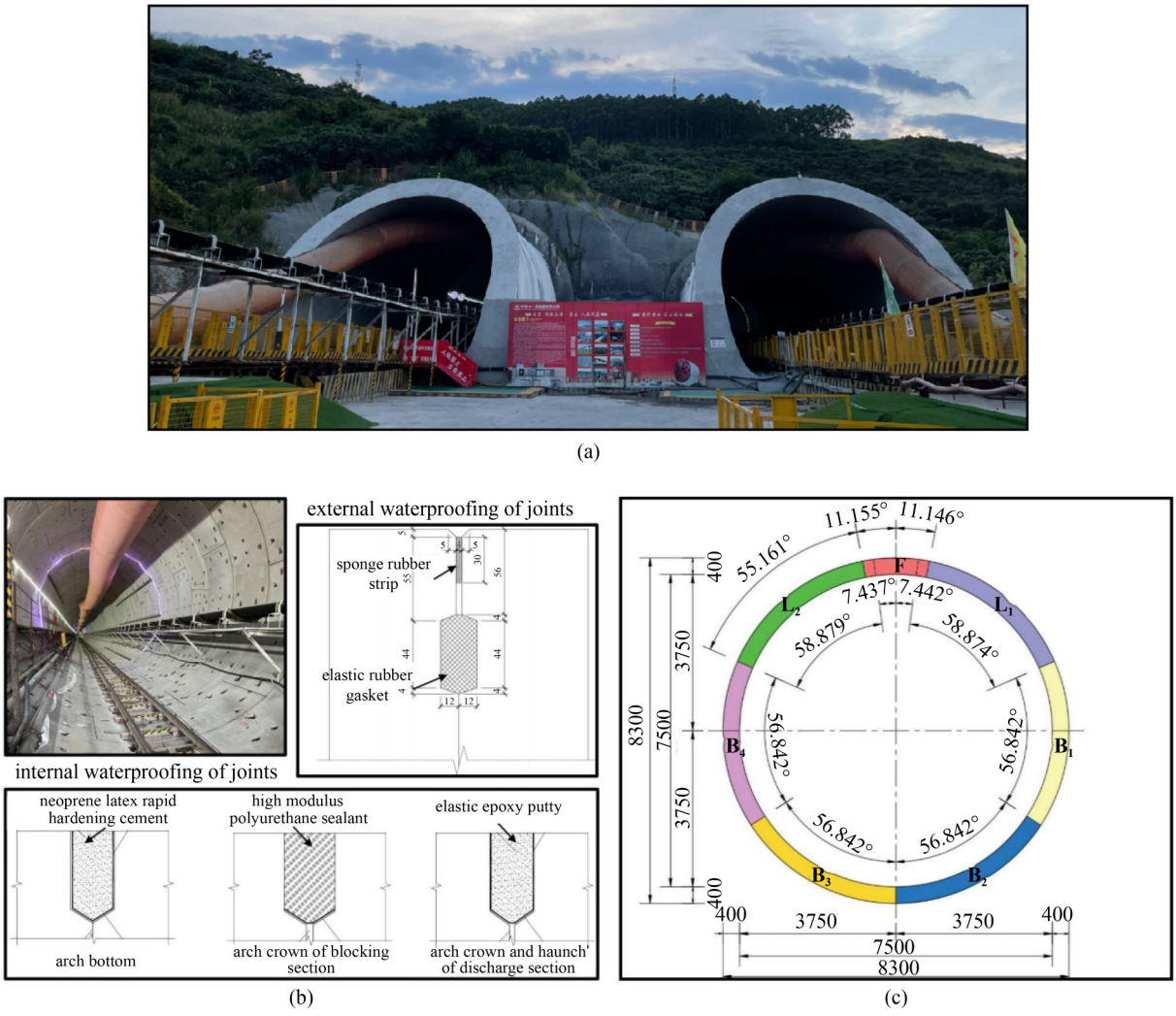

Fig. 4 Engineering conditions of the case study: (a) mountain tunnel under high water pressure; (b) TBM segments and waterproofing of the joint; (c) detailed dimensions of the segmental lining (unit: mm).

where H_w represents the distance from the groundwater level to the center of the tunnel; r_0 and r_1 represent the inner and outer radii of the second lining, respectively, which were both taken as half of the inner diameter D of the segmental lining in this study; r_2 and r_g represent the outer radii of the initial support and grouting ring, respectively; and k_s, k_i, k_g, and k_m are the permeability coefficients of the secondary lining, primary support, grouting, and surrounding rock, respectively.

According to Eq. (1), when the ratio of the grouting thickness d_g to r_0 is > 1, the reduction effect of radial grouting on Q_f and P is insignificant, as shown in Fig. 6. Thus, the thickness of the grouting ring was taken as r_0 to avoid wastage of construction materials [19]. In addition, the cross-sectional dimension of the drain holes was taken as 0.2 m × 0.2 m [21]. A pipe was used to represent the hole [27], and the porosity and permeability coefficient for drain holes and pinholes were taken as 1.5 and 0.2 m/s, respectively, to avoid the numerical singularity. The remaining parameters were set according to the geological survey report of the tunnel project and previous studies [17,23,28], as shown in Table 1.

3.2 Evolution of external water pressure of lining

3.2.1 Drain holes

To investigate the effects of the drain-hole arrangement in the longitudinal direction on the tunnel seepage field, the longitudinal number n_y of drain holes on one side of a single ring was taken as 0, 1, 2 (see Fig. 7(a)), and 3 within a length of 1.8 m (the width of a tunnel ring), assuming an inclination angle of θ_h = 45°, as shown in Fig. 2(a) [21,23]. Then, to investigate the evolution characteristics of the external water pressure of the lining, η was defined as the ratio of the water pressure of the segmental external surface to the limited external water pressure in Eq. (2). When η < 1, this type of drainage segment can significantly reduce the water pressure, and when η < 1, it cannot.

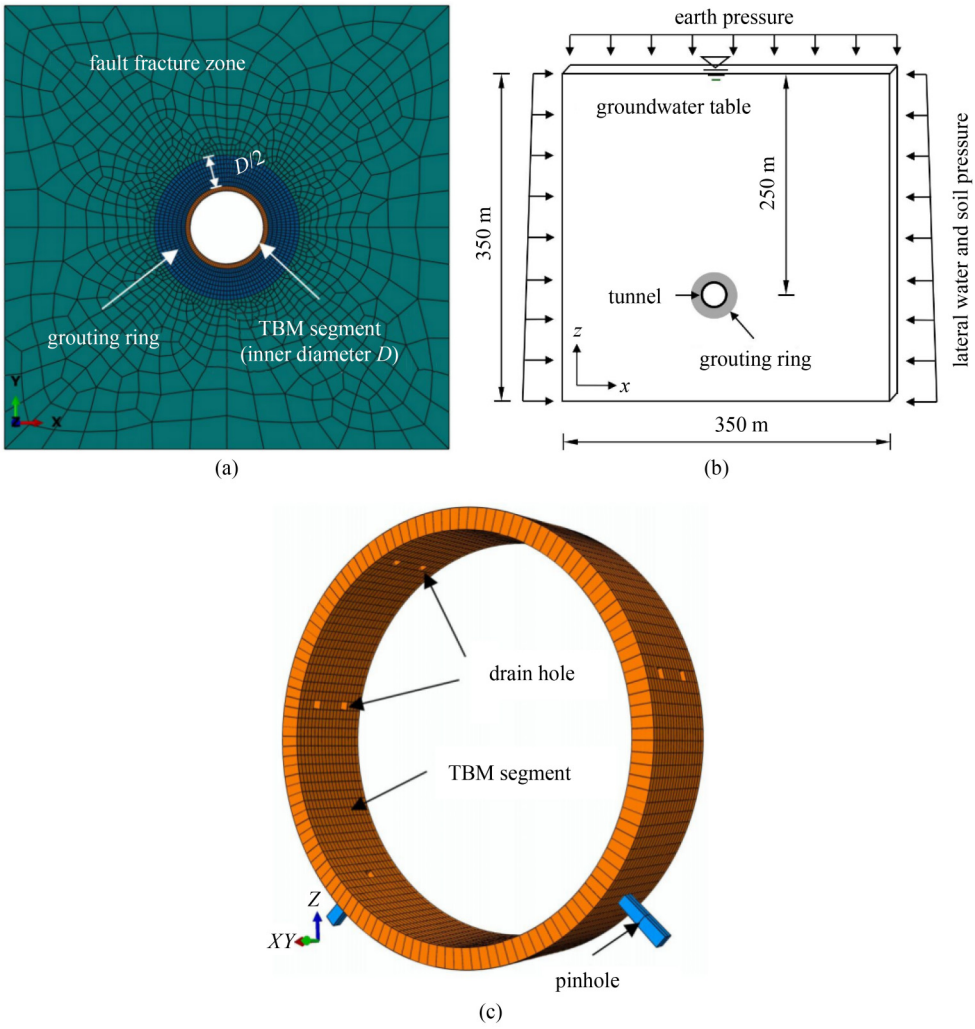

Fig. 5 Numerical model: (a) meshing of the partial model; (b) schematic of the overall model; (c) meshing of the segment and holes.

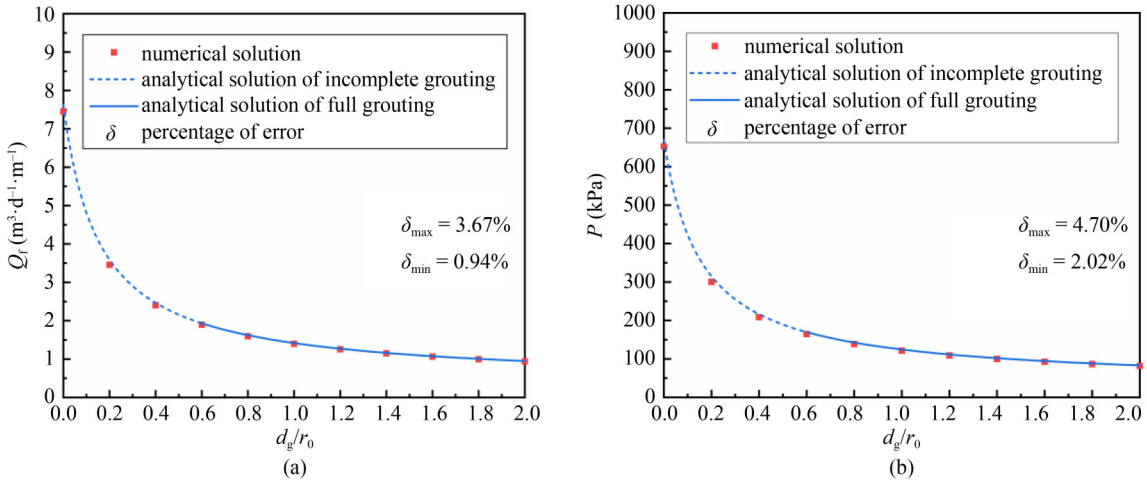

Fig. 6 Effect of the relative thickness of radial grouting on the seepage field. (a) Water inflow Q_f of tunnel face; (b) external water pressure P of arch crown.

$$\eta = \frac{P}{P_{\text{lim}}}, \tag{2}$$

where P represents the external water pressure of the lining, and P_{lim} represents the limit external water pressure value, which was 1.706 MPa for the project case [29].

By extracting the numerical calculation results and

Table 1 Parameter values

item	density, ρ (kg/m^3)	elastic modulus, E (GPa)	Poisson ratio, μ	cohesion, c (kPa)	friction angle, φ (°)	permeability coefficient, k (m/s)	porosity, n
fault fracture zone	2000	35.0	0.2	35	35	1×10^{-5}	0.2
grouting ring	2500	4.0	0.2	45	45	1×10^{-7}	0.5
segment	2500	35.5	0.2	–	–	1×10^{-12}	0.01
drain holes/pinholes	2500	35.5	0.2	–	–	0.2	1.5

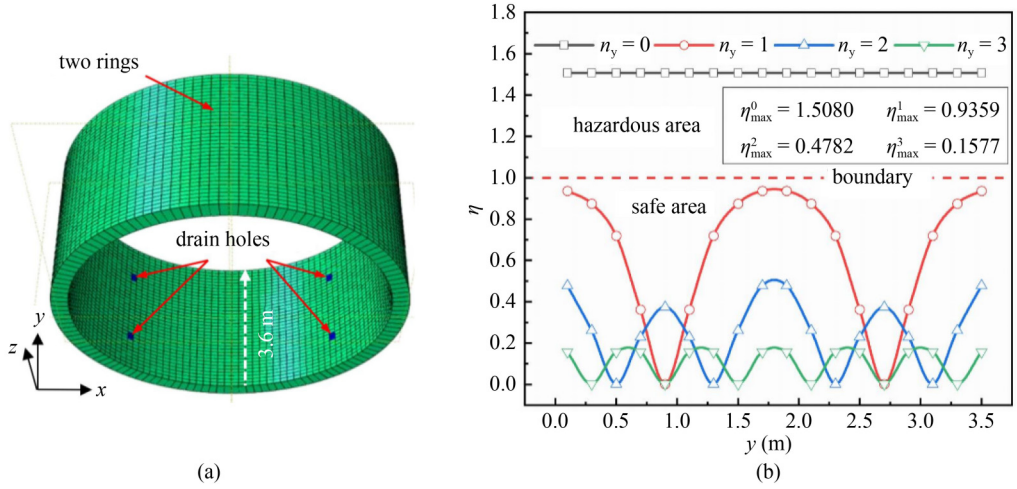

Fig. 7 (a) Arrangement of two segments along the longitudinal direction ($n_y = 2$, $n_\theta = 1$); (b) η–y curves under different n_y values ($\theta_h = 45°$).

processing the data, the η–y curves for different n_y values were obtained (see Fig. 7(b)), where y represents the distance along the longitudinal direction of the segment. The longitudinal external water pressure P was effectively reduced by the drain holes. Closer to the holes, the depressurization effect was more significant. When n_y increased from 0 to 1, η_{max} decreased by 37.94%. The amplitude of the single-hole pressure-reducing ratio was 37.94%. As n_y increased from 0 to 3, the amplitudes of the pressure-reducing ratio for the single-hole design were 34.14% and 29.85%, respectively. With an increase in n_y, the effect of the pressure reduction of the single hole was weakened. Even in the case of $n_y = 1$, P was in the safe range. Thus, the evolution law of the longitudinal external water pressure of the lining was not considered in the subsequent design analysis of the drainage segment.

Subsequently, the η–θ variation curves for different n_y values were obtained by extracting and processing the circumferential external water pressure P at joints between rings and drain holes, as shown in Fig. 8. θ_y was defined as the circumferential influence angle that effectively reduced P ($\eta < 1$), which is referred to as the pressure-reducing angle. It was obtained from the fitting function of Abaqus for the data points. A larger value of θ_y corresponded to a stronger pressure-reducing effect. Overall, as shown in Fig. 8, the P values at joints were larger than those at drain holes. The variation of η was the most significant near holes. This is because the P at the holes was 0, and the P values at the joints without holes were large. For protecting the segment structure, the subsequent drainage design focused on the evolution law of the external water pressure of the lining at circumferential joints.

We can infer from Fig. 8 that the pressure-reducing effect of the single hole was maximized at $n_y = 2$. Taking Fig. 8(a) as an example, the average pressure-reducing angles (θ_{avg}, i.e., the ratio of θ_y to the number of holes) of a single hole for n_y values of 1, 2, and 3 were 11.94°, 14.92°, and 11.67°, respectively. Comparing Figs. 8(a) and 8(b) revealed that as n_y increased, the difference in θ_y gradually decreased. There was no difference in θ_y until n_y reached 3. This indicated that when n_y reached a certain value, the drain hole had the same pressure-reducing effect on the circumferential area of the segment at all positions along the longitudinal direction.

Similarly, to investigate the effects of the arrangement in the lateral section on the groundwater environment, the circumferential number (n_θ) of drain holes on one side of a single ring was taken as 0, 1, 2, and 3, assuming $n_y = 2$. As indicated by the η–θ curves of Fig. 9, the circumferential external water pressure P decreased with an increase in n_θ, whereas θ_y exhibited the opposite trend. θ_{avg} increased by 10.92% when n_θ increased from 1 to 2. However, θ_{avg} increased by only 27.04% when n_θ increased from 2 to 3. Compared with the other two types, the

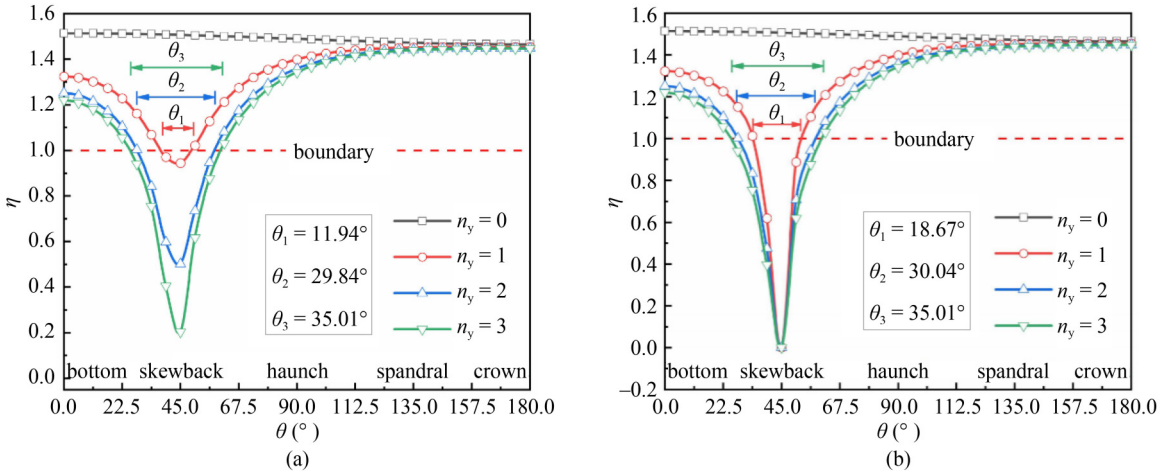

Fig. 8 η–θ curves for different n_y values ($\theta_h = 45°$). (a) Circumferential joints between rings; (b) drain holes.

triple-hole drainage-segment type was the most effective for reducing P. This may have been due to its combined pressure-reducing effect. For a smaller circumferential spacing angle of adjacent holes, this effect was more significant.

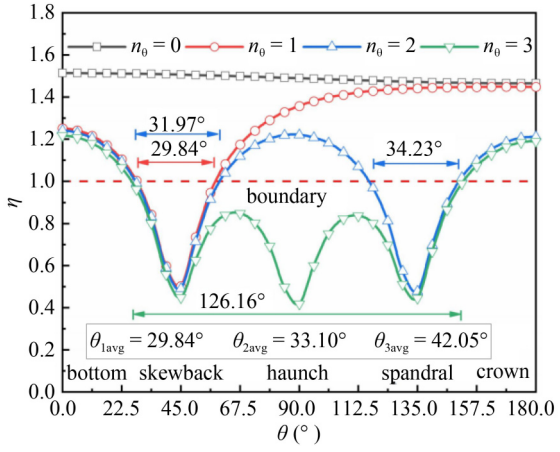

Fig. 9 η–θ curves for different n_θ values ($n_y = 2$, $y = 1.8$ m).

3.2.2 Pinholes

According to the principles of the limited and proximity discharge, pinholes were set near the arch bottom so that the groundwater can be directly discharged from the tunnel ditches. A three-dimensional numerical model of a tunnel seepage field subject to the non-constant water head, which was not considered in Refs. [18,19], was developed using the Abaqus software. The setting of a non-constant water head was implemented by changing the boundary conditions of the pore pressure in the geostatic, grouting, excavation, and segmental construction steps, i.e., the pore pressure at the groundwater-table line was set to 0. Subsequently, the lengths (L_{dh}) of the pinholes were taken as $0.25d_g$, $0.50d_g$, and $0.75d_g$, and the inclination angles (θ_{dh}) were taken as 30°, 45°, 60°, and 75°. For ease of discussion, the following parameters were defined.

$\theta_{0.25}$ was defined as the pressure-reducing angle with $L_{dh} = 0.25d_g$ ($\eta < 1$), and $\theta_{0.25}/180°$ was called the ratio of $\theta_{0.25}$ to the half-circle angle. The meanings of the parameters $\theta_{0.50}$ and $\theta_{0.75}$ were identical to those presented previously. $\beta_{0.25}$ was defined as the difference between the boundary value of η (taken as 1 in this study) and the η_0 at the arch bottom with $L_{dh} = 0.25d_g$, as given by Eq. (3). A smaller absolute value of $\beta_{0.25}$ implies that it is more reasonable for the drainage parameters of the pinholes to reduce P at the bottom. Similarly, the parameters $\beta_{0.50}$ and $\beta_{0.75}$ were defined. $\alpha_{0.25}$ was defined as the percentage that P of the arch crown was reduced by a certain pinhole type with $L_{dh} = 0.25d_g$, as given by Eq. (4). Similarly, the parameters $\alpha_{0.50}$ and $\alpha_{0.75}$ were defined.

$$\mu_{0.25} = 1 - \eta_0, \tag{3}$$

$$\alpha_{0.25} = \left(1 - \frac{\eta_{180}}{\eta_{180}^0}\right) \times 100\%, \tag{4}$$

where η_0 represents the ratio of the external water pressure of the lining to the limit external water pressure at the arch bottom, η_{180} represents the v of the arch crown of the drainage segment, and η_{180}^0 represents the η of the arch crown of the fully blocked segment.

The η–θ curves corresponding to different pinhole types were obtained for $y = 1.8$ m, as shown in Fig. 10. The η–θ curves exhibited a funnel-shaped distribution, where η gradually decreased when close to θ_{dh}. The η value gradually increased away from θ_{dh}. η was minimized at θ_{dh} and maximized at θ_{180}, satisfying $0° < \theta_{dh} < 90°$. Moreover, $\theta_{0.25}$, $\theta_{0.50}$, and $\theta_{0.75}$ increased with L_{dh}, and the increase gradually slowed. However, as θ_{dh} increased from 30° to 75°, $\theta_{0.25}$, $\theta_{0.50}$, and $\theta_{0.75}$ all exhibited a trend of first increasing and then decreasing. This indicated that

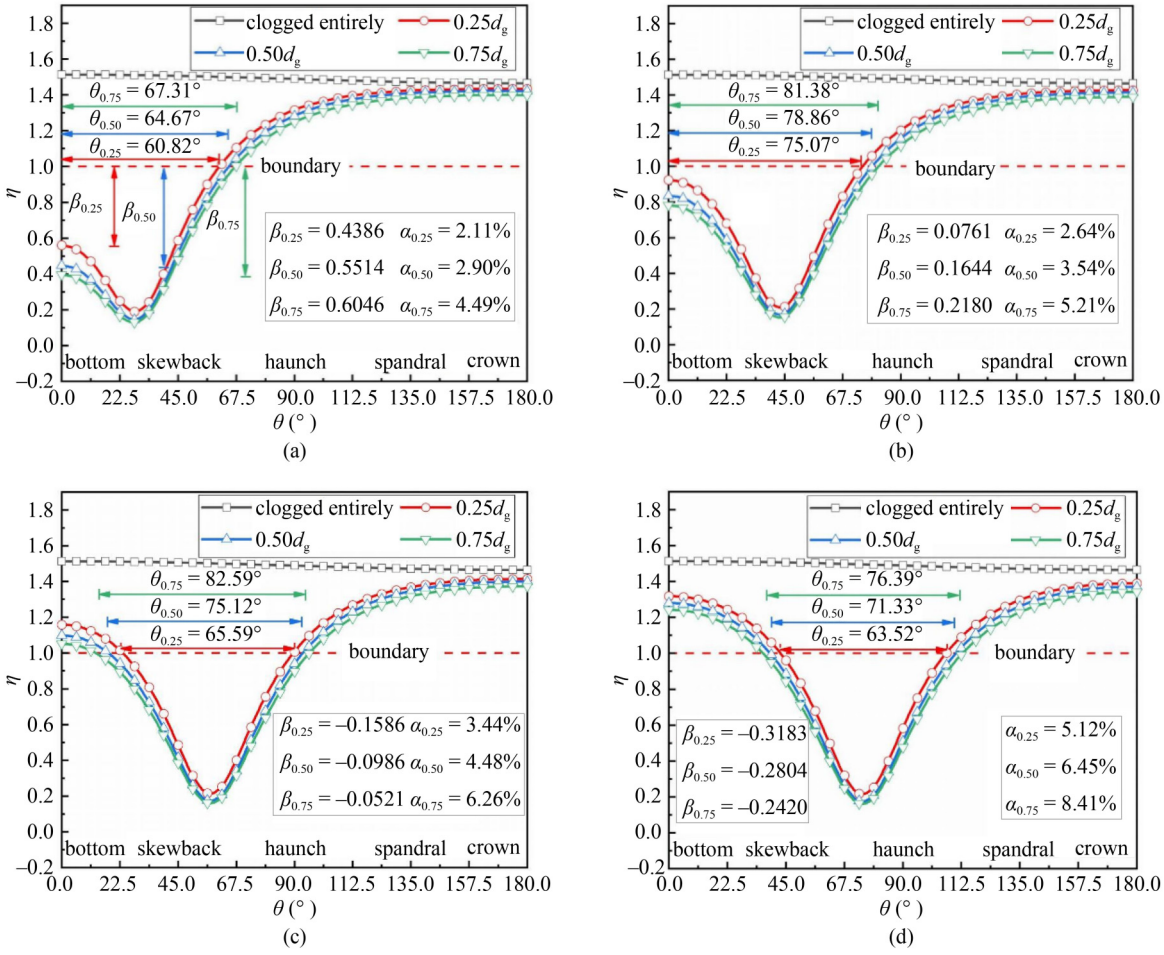

Fig. 10 η–θ curves for different pinhole types (y = 1.8 m). (a) θ_{dh} = 30°; (b) θ_{dh} = 45°; (c) θ_{dh} = 60°; (d) θ_{dh} = 75°.

for the pinhole drainage-segment design, there is an optimal inclination angle that results in the best pressure-reducing effect.

β also increased with L_{dh}, and its amplitude gradually decreased, as shown in Fig. 10. β was positive for $\theta_{dh} \leqslant$ 45°, indicating that the pinhole design significantly reduced the circumferential external water pressure P at the arch bottom. A smaller L_{dh} value corresponded to the P at the arch bottom being closer to the critical value, implying that the design parameters were more reasonable. In contrast, β was negative when θ_{dh} was $\geqslant$ 60°, which indicated that the pinhole type did not reduce the P in the bottom area of the segment to the safe range. The ideal pressure-reducing effect can be achieved by increasing L_{dh}, but this would significantly increase the discharge volume.

The parameter α increased with L_{dh} and θ_{dh}, and its amplitude increased gradually, as shown in Fig. 10. This indicated that for larger values of L_{dh} and θ_{dh}, the pin-hole design was more effective for reducing the P at the arch crown. Comparing the α values under different L_{dh} and θ_{dh} values revealed that the P at the arch crown was more sensitive to L_{dh} than to θ_{dh} when θ_{dh} was $\leqslant$ 45°. However, the P was more sensitive to θ_{dh} when θ_{dh} was $\geqslant$ 60°.

3.3 Evolution characteristics of segment discharge volume

3.3.1 Drain holes

As shown in Fig. 11, a statistical analysis was performed on the joint discharge volume of drain holes corresponding to the working conditions where n_y and n_θ were taken as 1, 2, and 3, respectively. With increases in n_y and n_θ, the discharge volume Q of the segment increased, and its amplitude gradually decreased. The maximum increase of the Q–n_y histogram was 45.83% when n_θ was fixed. However, when n_y was fixed, the maximum increase of the Q–n_θ histogram was 104.17%. Therefore, Q was far more sensitive to n_θ than to n_y. Additionally, as shown in Table 2, the average discharge volume of a single hole decreased with an increase in n_y when n_θ was the same. When n_y was the same, the average discharge volume of a single hole decreased with an increase in n_θ. Thus, a larger value of n_y corresponded

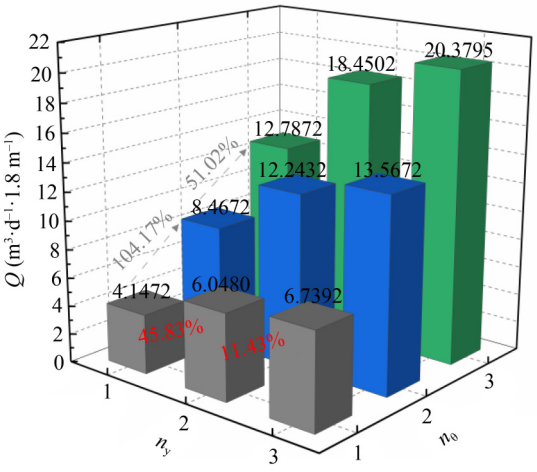

Fig. 11 Discharge volumes for different n_y and n_θ values.

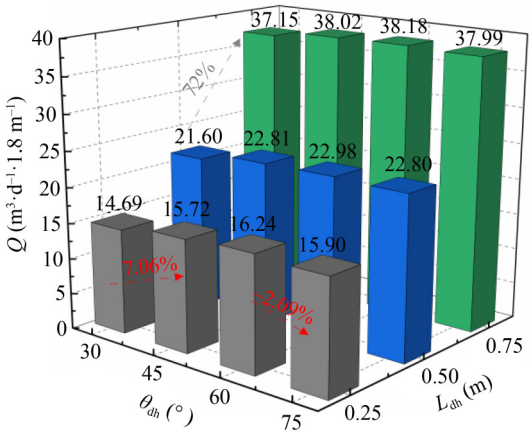

Fig. 12 Discharge volumes for different L_{dh} and θ_{dh} values.

Table 2 Average discharge volume per hole of the segment for different drainage types (m^3/d)

n_θ	$n_y = 1$	$n_y = 2$	$n_y = 3$
1	2.0736	1.5120	1.1232
2	2.1168	1.5304	1.1306
3	2.1312	1.5375	1.1322

to a smaller single-hole discharge capacity. The single-hole discharge capacity increased with n_θ.

3.3.2 Pinholes

Similarly, the histograms of the discharge volumes under different pinhole lengths (L_{dh} = 0.25d_g, 0.50d_g, and 0.75d_g) and inclination angles (θ_{dh} = 30°, 45°, 60°, and 75°) are shown in Fig. 12. When θ_{dh} was the same, Q increased with L_{dh}. Its maximum amplitude was 72.0%. In contrast, when L_{dh} was the same and θ_{dh} increased, Q first increased and then decreased. The maximum increase and decrease amplitudes were 7.06% and –2.09%, respectively. Under different L_{dh} values, Q was maximized at θ_{dh} = 60°. Thus, Q was far more sensitive to L_{dh} than to θ_{dh} for the pinhole drainage design. In actual tunnel engineering, the external water pressure of the lining in the lower part of the segment can be effectively reduced by setting pinholes at an inclination angle of approximately 60° and appropriately increasing their lengths.

3.4 Evolution of steady drawdown of groundwater table

3.4.1 Drain holes

After the tunnel seepage stabilized, a statistical analysis was performed on the groundwater-table drawdown, as shown in Table 3, for n_y and n_θ values of 1, 2, and 3. The groundwater-table drawdown increased with n_y and n_θ, and the increase gradually slowed. When n_θ was the same, the maximum increase in the amplitude of the drawdown with an increase in n_y was 45.83%. When n_y was the same, the maximum increase in amplitude of the drawdown with an increase in n_θ was 117.74%. These results were consistent with the evolution law of Q with respect to n_y and n_θ. This suggests that the discharge volume of the segment can be used as a quantitative index to determine the impact on the groundwater environment in the design of drain holes [5,20].

3.4.2 Pinholes

Similarly, a statistical analysis was performed on the groundwater-table drawdown under different pinhole lengths (L_{dh} = 0.25d_g, 0.50d_g, and 0.75d_g) and inclination angles (θ_{dh} = 30°, 45°, 60°, and 75°), as shown in Table 4. The drawdown increased with L_{dh}, whose maximum amplitude was 65.5%. As θ_{dh} increased from 30° to 75°, the drawdown first increased and then decreased. The maximum increase and decrease amplitudes were 5.81% and –1.03%, respectively. When θ_{dh} was 60°, the drawdown for different pinhole drainage types reached

Table 3 Groundwater-table drawdown for different n_y and n_θ values (m)

n_θ	$n_y = 1$	$n_y = 2$	$n_y = 3$
1	0.1883	0.2816	0.3245
2	0.4100	0.5723	0.6491
3	0.5405	0.7785	0.8851

Table 4 Groundwater-table drawdown for different L_{dh} and θ_{dh} values (m)

L_{dh}	θ_{dh} = 30°	θ_{dh} = 45°	θ_{dh} = 60°	θ_{dh} = 75°
0.25d_g	0.677	0.716	0.757	0.750
0.50d_g	1.000	1.043	1.069	1.058
0.75d_g	1.655	1.706	1.724	1.718

the maximum value. The drawdown was far more sensitive to L_{dh} than to θ_{dh}, and the evolution law was consistent with Q. This suggests that the discharge volume of the segment can be used as a quantitative index in the design of pinholes.

4 Results and discussion

4.1 Design parameter analysis

4.1.1 Drain holes

To reduce the impact of tunnel construction, the discharge volume of the segment and groundwater-table drawdown should be reduced. A wider effective pressure reduction range is better. Although there is no specification for the drawdown limit, the limit of the discharge volume can be determined by the capacity of the tunnel drainage system. Therefore, it is crucial to optimally balance the pressure-reducing range and the discharge volume.

The circumferential spacing angle of drain holes in the multi-hole drainage-segment designs is an important factor influencing the combined pressure-reducing effect of holes, which is expressed as $\Delta\theta_h$. The $\Delta\theta_h$ values of the circumferential double-hole and triple-hole drainage types are 90° and 45°, respectively. According to the findings of Subsubsection 3.2.1, the combined pressure-reducing effect of circumferential drain holes can reduce the external water pressure of the lining to within the safe range when $\Delta\theta_h = 45°$ and $n_y \geqslant 2$. Drain-hole segments with these design parameters have good applicability to high-water pressure tunnels.

The parameter λ_2 was defined as the ratio of the pressure-reducing angle ratio to the limit ratio of the discharge volume for $n_y = 2$, as given by Eq. (4), to evaluate the advantages and disadvantages of the aforementioned design parameters. The parameter λ_3 has the same meaning as above.

$$\lambda_2 = \frac{\theta_2}{180^\circ} \times \frac{Q_{lim}}{Q_2}, \tag{5}$$

where θ_2 (°) represents the pressure-reducing angle when $n_y = 2$, Q_2 ($m^3 \cdot d^{-1} \cdot 1.8^{-1}$ m^{-1}) represents the discharge volume of the segment when $n_y = 2$, and Q_{lim} ($m^3 \cdot d^{-1} \cdot 1.8^{-1}$ m^{-1}) represents the discharge volume limit of the segment, which was taken as 25 ($m^3 \cdot d^{-1} \cdot 1.8^{-1}$ m^{-1}) for the project case.

The pressure-reducing angle and discharge volume were substituted into Eq. (5) to obtain the λ values of the circumferential triple-hole segment at $n_y = 2$ and 3, as shown in Table 5. The λ value of $n_y = 2$ was 5.42% larger than that of $n_y = 3$ when $\Delta\theta_h$ was 45°. Thus, in the case of comprehensively considering the pressure-reducing range and discharge volume, the design parameters of the three-hole drainage type with $n_y = 2$ are reasonable.

4.1.2 Pinholes

Similarly, to quantitatively evaluate the advantages and disadvantages of the pinhole drainage design, $\lambda_{0.25}$ was defined as the ratio of the pressure-reducing angle ratio to the limit ratio of the discharge volume for $L_{dh} = 0.25d_g$ and $\beta_{0.25} \geqslant 0$, as given by Eq. (6). Similarly, the parameters $\lambda_{0.50}$ and $\lambda_{0.75}$ were defined.

$$\lambda_{0.25} = \frac{\theta_{0.25}}{180^\circ} \times \frac{Q_{lim}}{Q_{0.25}}, \tag{6}$$

where $\theta_{0.25}$ (°) represents the pressure-reducing angle when $L_{dh} = 0.25d_g$, and $Q_{0.25}$ ($m^3 \cdot d^{-1} \cdot 1.8^{-1}$ m^{-1}) represents the discharge volume of the segment when $L_{dh} = 0.25d_g$.

The β–θ curves were obtained by extracting the β values in Fig. 10 corresponding to $L_{dh} = 0.25d_g$, $0.50d_g$, and $0.75d_g$ to further determine the optimal inclination angle, as shown in Fig. 13. On the premise that β was $\geqslant 0$ (P was in the safe range), a smaller β value corresponded to the P at the arch bottom being closer to the limit value, indicating that the pinhole type is reasonable. In theory, the $\theta_{t\text{-}dh}$ corresponding to the L_{dh} of pinholes is the optimal inclination angle when the curve in Fig. 13 intersects the straight line. This parameter is referred to as the theoretical optimal inclination angle hereinafter. As shown in Fig. 13, the theoretical optimal inclination angles corresponding to $0.25d_g$, $0.50d_g$, and $0.75d_g$ were 47.25° ($\theta_{t\text{-}dh}^{0.25}$), 50.90° ($\theta_{t\text{-}dh}^{0.50}$), and 53.64° ($\theta_{t\text{-}dh}^{0.75}$),

Table 5 λ values at $n_y = 2$ and 3 ($\Delta\theta_h = 45°$)

n_y	$\theta/180°$	Q/Q_{lim}	λ
2	0.7009	0.7380	0.9497
3	0.7344	0.8152	0.9009

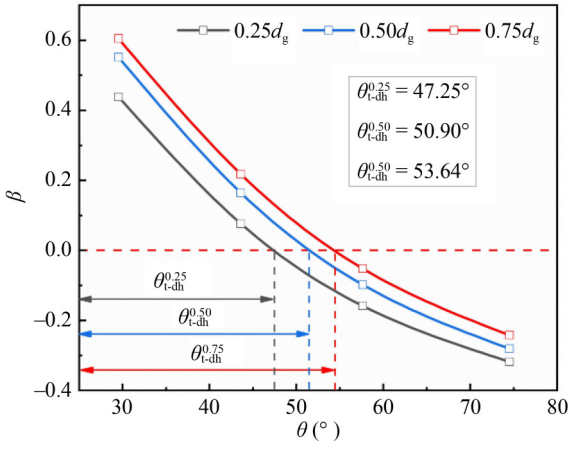

Fig. 13 β–θ curves of pinholes for different L_{dh} values.

respectively.

However, the inclination angles of the numerical simulation were not completely consistent with the theoretical optimal inclination angles, owing to the mesh division. Thus, on the premise of ensuring $\beta > 0$, a numerical inclination angle close to the theoretical optimal inclination angle was selected. According to the numerical calculations performed in this study, the optimal inclination angles corresponding to $0.25d_g$, $0.50d_g$, and $0.75d_g$ were selected as 47.25° ($\theta_{dh}^{0.25}$), 50.90° ($\theta_{dh}^{0.50}$), and 53.64° ($\theta_{dh}^{0.75}$), respectively. The curves for the three optimization types of pinholes are shown in Fig. 14, where L_{dh} and the corresponding θ_{dh} were taken as improved parameters. The β values for the three optimized pinhole types were all < 0.05, indicating that the above design parameters were reasonable. The pressure-reducing angles of the three curves all increased with L_{dh}, and the increase gradually slowed. However, a single factor was insufficient for comprehensively evaluating the advantages and disadvantages of the drainage design; thus, further evaluation was performed using the λ value (see Table 6).

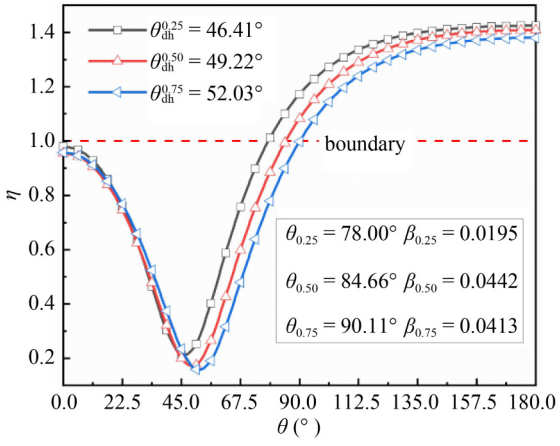

Fig. 14 η–θ curves for different pinhole designs.

Table 6 λ values for three optimized designs of pinholes

parameter	$\theta_{dh}^{0.25}$ = 46.41°	$\theta_{dh}^{0.50}$ = 49.22°	$\theta_{dh}^{0.75}$ = 52.03°
θ/180°	0.4333	0.4703	0.5006
Q/Q_{lim}	0.6290	0.9124	1.5552
λ	0.6889	0.5155	0.3219

As indicated by Table 6, the θ/180° values of the three optimized pinhole types increased with L_{dh}, whose amplitude gradually decreased. The maximum increase amplitude was 8.54%. Additionally, Q/Q_{lim} increased with L_{dh}, and its amplitude increased gradually. The maximum increase amplitude was 70.45%. These results indicated that the discharge volume was far more sensitive to L_{dh} than the pressure-reducing angle. The λ value decreased with an increase in L_{dh}, and the decrease rate gradually increased. With comprehensive consideration of the pressure-reducing range and discharge volume in the lower part of the segment, the optimal design parameters of pinholes were determined to be $L_{dh} = 0.25d_g$ and $\theta_{dh}^{0.25} = 46.41°$.

4.2 Design consideration of combined drainage segments for TBM tunnels under high water pressure

4.2.1 Selection of design parameters

The optimal parameters of pinholes in the lower part of the segment were determined as described in Subsubsection 4.1.2, and the corresponding pressure-reducing angle was 78° (see Fig. 14). We deduced that the pressure-reducing angle of drain holes in the upper part of the segment should be ⩾ 102°. On the basis of the related data in Fig. 9, a statistical table of the total pressure-reducing angle under different design parameters of drain holes is presented in Table 7. The maximum total pressure-reducing angles for the circumferential single-hole and double-hole types were 35.01° and 78.01°, respectively. Neither satisfies the design requirement of the combined drainage segment. However, the total pressure-reducing angles for the circumferential triple-hole type were 126.16° and 132.19° for n_y = 2 and 3, respectively, satisfying the requirement of > 102°. These results provide guidance for the selection and optimization of design parameters.

Table 7 Total pressure-reducing angles under different design parameters of drain holes (°)

n_y	$n_\theta = 1$	$n_\theta = 2$ ($\Delta\theta_h = 90°$)	$n_\theta = 3$ ($\Delta\theta_h = 45°$)
1	11.94	29.80	81.13
2	29.84	66.20	126.16
3	35.01	78.01	132.19

The parameter κ was defined as the difference between η (taking 1) and η_{max} (within the range of θ_{h1} to θ_{h2}) to facilitate the selection, as given by Eq. (7). It quantifies the combined pressure-reducing effect between circumferential drain holes. $\kappa > 0$ indicates that the P in the area between drain holes is reduced to within the safe range. A larger κ value corresponds to a more significant pressure-reducing effect.

$$\kappa = 1 - \eta_{max}. \tag{7}$$

Taking the circumferential triple-hole type ($\Delta\theta_h = 45°$) in Fig. 8 as the standard type, the η–θ curves for different n_y values are shown in Fig. 15. Here, the combined pressure-reducing effect of the holes is clearly observed. The P value of the area between two holes was effectively reduced to within the safe range when κ was > 0 for n_y = 2 and 3. In contrast, when κ was < 0 under the

condition of $n_y = 1$, the P in the local area between holes could not be reduced to within the safe range. Referring to the κ value for the standard type ($\Delta\theta_h = 45°$), the rationality of the design parameters of drain holes was determined. As shown in Table 8, $\Delta\theta_h > 45°$ for Design A indicates that the combined pressure-reducing effect between holes is worse than that for the standard type. Thus, the corresponding δ value should be > 0 to enhance the pressure-reduction effect. It is reasonable to select $n_y = 2$. $\Delta\theta_h < 45°$ in Design B indicates that the combined pressure-reducing effect between holes is better than that for the standard type. Accordingly, the κ value should be < 0 to avoid excessive pressure reduction. An n_y value of 1 is reasonable. In summary, reasonable design parameters of drain holes for the combined drainage type are $\Delta\theta_h = 51°$, $n_y = 2$ or $\Delta\theta_h = 34°$, and $n_y = 1$.

4.2.2 Selection of segment schemes

According to the analysis results of Subsubsections 4.1.2 and 4.2.1, correspondingly, the combined drainage segment also has two design types (referred to as Designs A and B), as shown in Fig. 16. The η–θ curves obtained by extracting the circumferential external water pressure P are shown in Fig. 17. Designs A and B reduced the P of the entire ring to within the safe range, indicating that both types satisfy the basic drainage requirements. The parameter λ was used to quantitatively evaluate the advantages and disadvantages of Designs A and B. After the data were processed, the $\theta/180°$, Q/Q_{lim}, and λ values were obtained, as shown in Table 9.

As shown in Table 9, the pressure-reducing ranges of the two new drainage segments were identical. The Q/Q_{lim} of Design A is 11.20% smaller than that of Design B, but the λ value of Design A is 12.61% larger than that of Design B. Considering the pressure-reducing range and discharge volume comprehensively, Design A is better. Regarding the number of holes on one side of a single ring, Design A has 2 more holes than Design B; i.e., the number of holes is increased by 25%, but the λ value is only increased by 12.61%. From this viewpoint, it appears that Design A did not achieve the expected drainage effect. However, the drain holes and pinholes in Design A are not distributed along the same longitudinal axis, and the holes have less impact on the safety of the

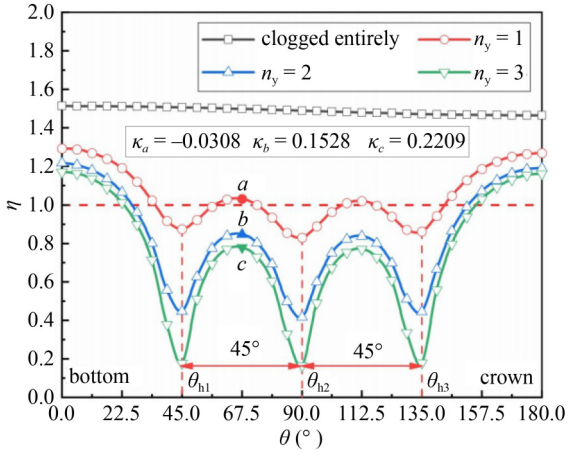

Fig. 15 η–θ curves of the trial-hole drainage segment for different n_y values ($\Delta\theta_h = 45°$).

Table 8 Table for the design types of drain holes

drain type	range angle (°)	n_θ	$\Delta\theta_h$ (°)	κ		
				$n_y = 1$	$n_y = 2$	$n_y = 3$
standard type	180	3	45	–0.0308	0.1528	0.2209
Design A	102	2	51	–	reasonable	–
Design B	102	3	34	reasonable	–	–

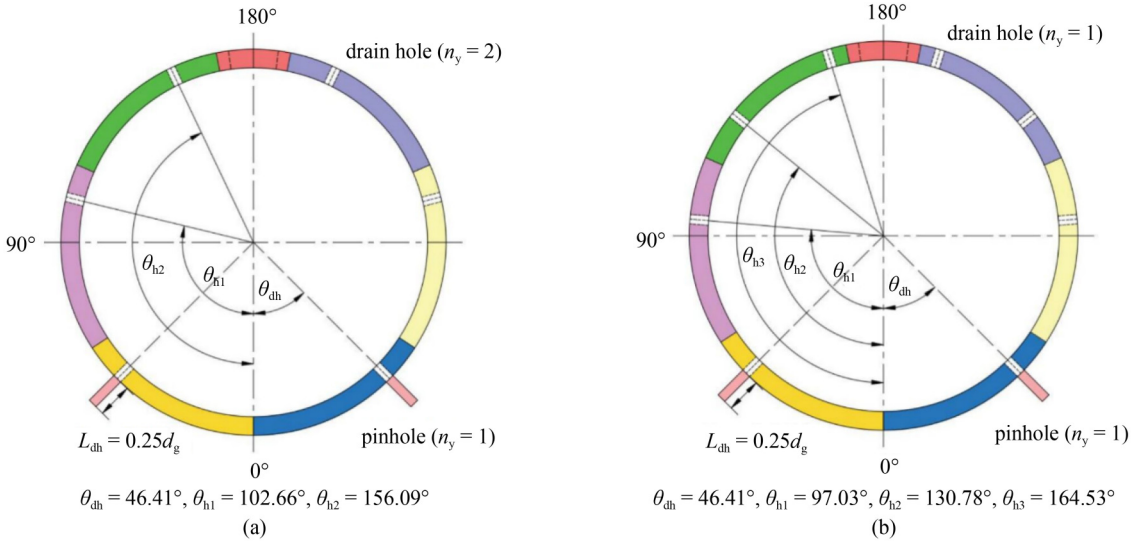

Fig. 16 New combined drainage types (A and B) of TBM segments. (a) Design A; (d) Design B.

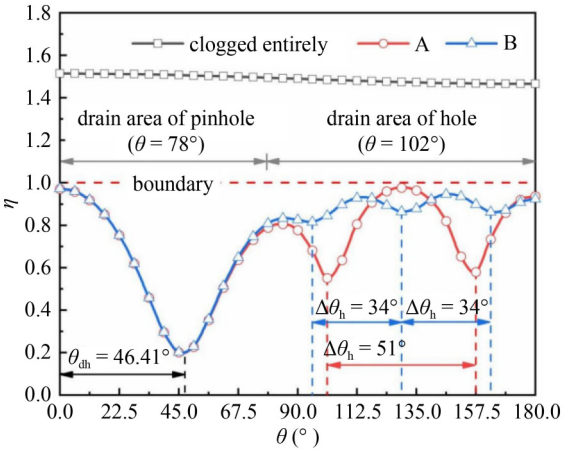

Fig. 17 η–θ curves of Designs A and B ($\Delta\theta_h = 45°$).

Table 9 λ values of Designs A and B

new type	$\theta/180°$	Q/Q_{lim}	λ
Design A	1	0.8225	1.2158
Design B	1	0.9262	1.0797

segment structure. The drain holes and pinholes of Design B are distributed at $y = 0.9$ m, where the segment structure is more prone to shear failure under the external force. Thus, the drainage parameters of Design A are more reasonable.

Moreover, the long-term behaviors of the tunnel lining must be monitored and assessed before actual project application [13]. Laboratory model tests (similar to Refs. [22,30]) should be performed. With the introduction of new materials, glass fiber-reinforced plastic has an ultimate stress value of 600–700 MPa and better economy [18]. It also makes the application of the novel drainage segment in seawater more feasible. Additionally, the effects of the segmental lining parameters (e.g., permeability and thickness), permeability of the grouting layer, and buried depth of the tunnels, should be considered. Research on the groundwater pollution, drying of springs, and wilting of surface vegetation should be conducted to improve the design parameters for the proposed drainage type.

5 Conclusions

The evolution characteristics, including the external water pressure and discharge volume of the segmental lining and the groundwater-table drawdown, were studied for drain holes and pinholes via numerical modeling. A new drainage design method for TBM segments was proposed, which exploits the advantages of drain holes and pinholes. The following conclusions are drawn.

1) For drain-hole drainage segments, the pressure-reducing angle, discharge volume, and groundwater-table drawdown increase with an increase in n_y in the longitudinal direction. They decrease with an increase in $\Delta\theta_h$ in the lateral direction. The discharge volume and groundwater-table drawdown are far more sensitive to $\Delta\theta_h$ than to n_y. The discharge capacity of a single hole decreases with increases in n_y and $\Delta\theta_h$. Considering the circumferential pressure-reducing range and discharge volume, the optimal design parameters of drain holes are $\Delta\theta_h = 45°$ and $n_y = 2$.

2) For pinhole drainage segments, the pressure-reducing angle, discharge volume, and groundwater-table drawdown increase with L_{dh}. With an increase in θ_{dh}, they first increase and then decrease. For the segments with different L_{dh} values, therefore, an optimal θ_{dh} exists. The discharge volume and groundwater-table drawdown are far more sensitive to L_{dh} than to θ_{dh}. The optimal design parameters of pinholes are $L_{dh} = 0.25d_g$ and $\theta_{dh}^{0.25} = 46.41°$.

3) The proposed combined discharge type of TBM segments controls the external water pressure in the lower area of tunnel rings through pinholes near the arch bottom. Additionally, a certain number of drain holes are arranged between the haunch and the crown to control the external water pressure in the upper area. The groundwater near pinholes can be quickly discharged through the tunnel ditches, and other groundwater can be diverted and discharged through the drain holes. A mountain tunnel under a high water pressure was taken as a project case, and the optimal design parameters of the proposed drainage segment were $\Delta\theta_h = 51°$, $n_y = 2$, $L_{dh} = 0.25d_g$, and $\theta_{dh}^{0.25} = 46.41°$.

A fluid–structure coupling analysis for TBM drainage segments was performed using the pore fluid-stress elements in Abaqus. The main objects simulated were segments and holes, for investigating the evolution law of the groundwater environment under different drainage types. The results indicated that the circumferential arrangement of the combined drainage type can exploit the advantages of drain holes and pinholes. The effect of the internal and external waterproofing measures of the longitudinal joints between segments and circumferential joints between rings shown in Fig. 4(b) was regarded as ideal. Then, two rings were regarded as a single ring to increase the efficiency of the numerical calculation. Recently, the DFLOW subroutine was developed to simulate the seepage characteristics of segmental joints in Abaqus [31]. This study focused on the effects of the seepage rate of the joints on the internal force and settlement of the tunnel structure in the operation stage. It provides valuable guidance for detailed simulation of the hydromechanical behavior of segmental joints.

Acknowledgements This work was supported by the National Natural Science Foundation of China (Grant No. 41972276), the Natural Science

Foundation of Fujian Province (No. 2020J06013), and the "Foal Eagle Program" Youth Top-notch Talent Project of Fujian Province (No. 00387088). The financial support is gratefully acknowledged.

Conflict of Interest The authors declare that they have no conflict of interest.

References

1. Liu J, Liu D, Song K. Evaluation of the influence caused by tunnel construction on groundwater environment: A case study of tongluoshan tunnel, China. Advances in Materials Science and Engineering, 2015: 149265
2. Wang G F, Wu Y X, Lu L H, Li G, Shen J S. Investigation of the geological and hydrogeological environment with relation to metro system construction in Jinan, China. Bulletin of Engineering Geology and the Environment, 2019, 78(2): 1005−1024
3. Chen S, Peng H Y, Yang C, Chen B L, Chen L C. Investigation of the impacts of tunnel excavation on karst groundwater and dependent geo-environment using hydrological observation and numerical simulation: A case from karst anticline mountains of southeastern Sichuan Basin, China. Environmental Science and Pollution Research International, 2021, 28(30): 40203−40216
4. Mossmark F, Annertz K K, Ericsson L O, Norin M. Hydrochemical impact of construction of the western section of the Hallandsås rail tunnel in Sweden. Bulletin of Engineering Geology and the Environment, 2017, 76(2): 751−769
5. Cheng P, Zhao L H, Luo Z B, Li L, Li Q, Deng X, Peng W Q. Analytical solution for the limiting drainage of a mountain tunnel based on area-well theory. Tunnelling and Underground Space Technology, 2019, 84: 22−30
6. Yu J Y, Ge S S, Hou L C, Zhang Y T, Liu Y Z. Limit drainage of separated tunnel based on ecological groundwater table: A case study. Advances in Civil Engineering, 2021: 2669924
7. Gokdemir C, Rubin Y, Li X J, Xu H. A vulnerability assessment method to evaluate the impact of tunnel drainage on terrestrial vegetation under various atmospheric and climatic conditions. Advances in Water Resources, 2021, 147: 103796
8. Lv Y X, Jiang Y J, Hu W, Cao M, Mao Y. A review of the effects of tunnel excavation on the hydrology, ecology, and environment in karst areas: Current status, challenges, and perspectives. Journal of Hydrology, 2020, 586: 124891
9. Lee S, Moon J S. Excessive groundwater inflow during TBM tunneling in limestone formation. Tunnelling and Underground Space Technology, 2020, 96: 103217
10. Aalianvari A, Katibeh H, Sharifzadeh M. Application of fuzzy Delphi AHP method for the estimation and classification of Ghomrud tunnel from groundwater flow hazard. Arabian Journal of Geosciences, 2012, 5(2): 275−284
11. Gattinoni P, Scesi L. The groundwater rise in the urban area of Milan (Italy) and its interactions with underground structures and infrastructures. Tunnelling and Underground Space Technology, 2017, 62: 103−114
12. Colombo L, Gattinoni P, Scesi L. Stochastic modelling of groundwater flow for hazard assessment along the underground infrastructures in Milan (northern Italy). Tunnelling and Underground Space Technology, 2018, 79: 110−120
13. Zhou Z, Zhang J J, Gong C J. Automatic detection method of tunnel lining multi-defects via an enhanced You Only Look Once v4 network. Computer-Aided Civil and Infrastructure Engineering, 2022, 37(6): 762−780
14. Cheng P, Zhao L H, Li L, Zou J F, Luo W. Limiting drainage criterion for groundwater of mountain tunnel. Journal of Central South University, 2014, 21(12): 4660−4668
15. Liu B, Wang Y X, Zhao G Z, Yang B, Wang R R, Huang D X, Xiang B. Intelligent decision method for main control parameters of tunnel boring machine based on multi-objective optimization of excavation efficiency and cost. Tunnelling and Underground Space Technology, 2021, 116: 104054
16. Xu Z H, Wang W Y, Lin P, Nie L C, Wu J, Li Z M. Hard-rock TBM jamming subject to adverse geological conditions: Influencing factor, hazard mode and a case study of Gaoligongshan Tunnel. Tunnelling and Underground Space Technology, 2021, 108: 103683
17. Shin H S, Youn D J, Chae S E, Shin J H. Effective control of pore water pressures on tunnel linings using pin-hole drain method. Tunnelling and Underground Space Technology, 2009, 24(5): 555−561
18. Kim D R, Kim H J, Shin J H. Performance evaluation of pin-holed pipe anchor for fractured zone in subsea tunnel. Marine Georesources and Geotechnology, 2017, 35(6): 769−779
19. Zhang Z J, Zeng C P, Li H, Gao Y, Gong L, Li Y X, Liang H F, Zhang E Z. Optimal design of the seepage control for Xianglushan diversion tunnel under high external water pressure. Geotechnical and Geological Engineering, 2022, 40(9): 4595−4615
20. Yan Q X, Ma T T, Chen F. Study of influence of water discharge volume on lining external loads for discharge segment lining. Rock and Soil Mechanics, 2011, 32(4): 1108−1112 (in Chinese)
21. Yan Q X, Cheng X, Zheng J, He C. Analysis on fluid−structure interaction of drainage segment lining under different drainage schemes. Journal of the China Railway Society, 2012, 34(6): 95−100 (in Chinese)
22. Yan Q X, Zhang M, Cheng X. Study of model test for water pressure distribution character behind drainage segment lining. Chinese Journal of Rock Mechanics and Engineering, 2013, 32(S1): 2617−2623 (in Chinese)
23. Qi C. Study on mechanical characteristics of segmental lining structure for deep-buried inclined shaft constructed by shield. Dissertation for the Doctoral Degree. Chengdu: Southwest Jiaotong University, 2017 (in Chinese)
24. Afshani A, Li W, Oka S, Itoh Y, Akagi H. Study of the long-term behavior of segmented tunnels in cohesive soil based on the circumferential joint opening. Tunnelling and Underground Space Technology, 2022, 120: 104210
25. GB 50164-2011. Chinese Standard for Quality Control of Concrete. Beijing: China Architecture Publishing & Media Co., Ltd., 2011, 9−10
26. Li P F, Wang F, Long Y Y, Zhao X. Investigation of steady water inflow into a subsea grouted tunnel. Tunnelling and Underground Space Technology, 2018, 80: 92−102
27. Li L Y, Yang J S, Wang L C, Wang S Y, Fang X H, Xie Y P.

Cause analysis and treatment measures of the inverted arch heaving disease of a high-speed railway tunnel under heavy rainfall. Modern Tunnelling Technology, 2021, 58(1): 27−36

28. Zhao T C, Han T R, Wu G, Gao Y, Lu Y. Effects of grouting in reducing excessive tunnel lining deformation: Field experiment and numerical modelling using material point method. Tunnelling and Underground Space Technology, 2021, 116: 104114
29. Arnau O, Molins C. Theoretical and numerical analysis of the three-dimensional response of segmental tunnel linings subjected to localized loads. Tunnelling and Underground Space Technology, 2015, 49: 384−399
30. Wang S C, Jiang X, Bai Y. The influence of hand hole on the ultimate strength and crack pattern of shield tunnel segment joints by scaled model test. Frontiers of Structural and Civil Engineering, 2019, 13(5): 1200−1213
31. Gong C J, Wang Y Y, Peng Y C, Ding W Q, Lei M F, Da Z, Shi C H. Three-dimensional coupled hydromechanical analysis of localized joint leakage in segmental tunnel linings. Tunnelling and Underground Space Technology, 2022, 130: 104726